

GSOFA: Scalable Sparse LU Symbolic Factorization on GPUs

Anil Gaihre
Stevens Institute of Technology

Xiaoye S. Li *
*Lawrence Berkeley National Laboratory

Abstract—Decomposing a matrix A into a lower matrix L and an upper matrix U , which is also known as LU decomposition, is an important operation in numerical linear algebra. For a sparse matrix, LU decomposition often introduces more nonzero entries in the L and U factors than the original matrix. *Symbolic factorization* step is needed to identify the nonzero structures of L and U matrices. Attracted by the enormous potentials of Graphics Processing Units (GPUs), an array of efforts has surged to deploy various steps of LU factorization on GPUs except, to the best of our knowledge, symbolic factorization. This paper introduces GSOFA, a GPU based symbolic factorization design with the following three optimizations to enable scalable LU symbolic factorization for *nonsymmetric pattern* sparse matrices on GPUs. First, we introduce a novel fine-grained parallel symbolic factorization algorithm that is well suited for the *Single Instruction Multiple Thread* (SIMT) architecture of GPUs. Second, we propose multi-source concurrent symbolic factorization to improve the utilization of GPUs with focus on balancing the workload. Third, we introduce a three-pronged optimization to reduce the excessive space requirement faced by multi-source concurrent symbolic factorization. Taken together, this work scales LU symbolic factorization towards 1,000 GPUs with superior performance over the state-of-the-art CPU algorithm.

I. INTRODUCTION

Many scientific and engineering problems require solving large-scale linear systems, $Ax = b$. Solving this problem with direct methods [7] often involves LU factorization, that is, decomposing the original matrix A into lower and upper triangular matrices L and U , respectively, where $A = LU$. Since LU decomposition of a sparse matrix typically introduces more nonzeros, also referred to as fill-in, than the original matrix A , as shown in Figure 1(a), *symbolic factorization* is designed to compute the structure of these nonzeros for both L and U . This information is subsequently used to predict the essential memory space for the subsequent numerical factorization. For brevity, we defer the discussion of other major steps of LU factorization to Section II-A.

Reviewing literature, we find two, if not more, problems that prevent the existing algorithms from scaling symbolic factorization on GPUs, i.e., data dependency and lack of fine-grained parallelism. Particularly, there exist two well-known symbolic factorization algorithms, that is, *fill1* and *fill2* [44], both of which identify a fill-in at $(L + U)[v][w]$ if and only if there exists a directed path from vertex v to w , with the intermediate vertices smaller than both v and w , where v and w can be any pair of vertices in the graph representation of A , i.e., $G(A)$. The main difference lies in that *fill1* computes the fill-in structure using the partially computed L and U while *fill2* relies upon the original A . To aid the understanding,

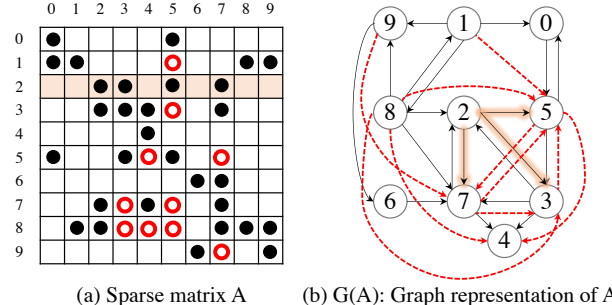


Figure 1: (a) Sparse matrix A and its (b) Graph representation $G(A)$. In (a), \bullet and \circ are, respectively, the original and new nonzeros (fill-ins) in L & U factored matrices. Accordingly, (b) uses \rightarrow and \dashrightarrow to indicate the original and new edges, respectively, in the L & U graphs. Note, diagonal non-zeros of (a) are self edges in (b) which are omitted for brevity.

Figure 1(b) depicts the graph representation $G(A)$ for the sparse matrix A in Figure 1(a). Particularly, each row of matrix A corresponds to a vertex in the graph $G(A)$ with every column of that specific row corresponds to an out edge of that vertex. For instance, row 2 of A in Figure 1(a) has non-zeros in columns $\{2, 3, 5, 7\}$. We thus have those corresponding out edges for vertex 2 in $G(A)$ of Figure 1(b), except the self edge. We will use this example throughout this paper.

The data dependency problem mainly occurs in the *fill1* algorithm, which was used in [24], [34], [37]. This algorithm is enhanced by several optimization techniques such as symmetric pruning [17] and supernode [9], [45], [3]. However, the *fill1* algorithm presents stringent synchronization requirements in the following two ways. First, the detection of the fill-ins for the current row or column also depends upon the fill-ins of the prior rows or columns, which introduces communication overhead. Second, we observe that, although symmetric pruning and supernode can help reduce the amount of computation, they come with nontrivial communication overhead, which is extremely costly when scaling to 1,000 GPUs. We also notice that separator tree [25] can help dissect the matrix A into independent rows/columns so that the independent ones can be processed without the updates from each other. However, such type of optimizations are problem dependent.

While data dependency problem can be addressed by switching to *fill2* algorithm, the lack of *fine-grained* parallelism of both *fill1* and *fill2* algorithms [44], as well as the other variants [5], [25], [17] is the roadblock that makes it hard to effectively utilize the GPU resources. Particularly,

fill2 algorithm can work on multiple sources in parallel, but each source is only allowed to work on one neighbor at a time. One might allow different GPU threads to work on dissimilar sources concurrently, but this design will cause warp divergence, strided memory access and overwhelming memory consumption. In summary, this algorithm exposes only coarse-grained parallelism which cannot fit the SIMD architecture of GPUs. It is also important to note that simply allowing fill2 to process multiple vertices in parallel will *not* warrant the correctness (discussed in Challenge#1 of Section III).

This paper, countering the traditional wisdom, chooses the fill2 algorithm as a base to develop scalable symbolic factorization. In order to enable GPU-based symbolic factorization, we revamp the fill2 algorithm to exhibit fine-grained parallelism. Taken together, **gSofa** can scale beyond 1,000 GPUs with unprecedented performance. Overall, this paper makes the following contributions.

First, to the best of our knowledge, we introduce the first, fine-grained parallel symbolic factorization that is well suited for the SIMD architecture of GPUs. Instead of processing one vertex at a time, we allow all the neighboring vertices to be processed in parallel, such that computations align well with the SIMD nature. *Since this relaxation allows some vertices to be traversed before their dependencies are satisfied, we further allow re-visitations of these vertices to ensure correctness.* We also introduce optimizations to reduce the re-initialization overhead and random memory access to algorithmic data.

Second, since one source often fails to saturate the entire GPU, we introduce multi-source concurrent symbolic factorization to improve the utilization of GPUs. *While multi-source traversal is not invented by this work, we resolve a fundamentally different challenge*, that is workload imbalance, instead of irregular memory access pattern from prior attempts [47], [36]. Particularly, we introduce two strategies to tackle intra- and inter- GPU workload imbalance problems, respectively. For the former problem, we use combined traversal to allow various GPU threads to work on active vertices irrespective to their sources. For the latter issue, we propose to interleave the source assignment to various GPUs in order to balance the workload across GPUs.

Third, we introduce a three-pronged optimization to combat the excessive space consumption problem faced by multi-source concurrent symbolic factorization. First, we propose the out-of-core¹ frontier management because the space requirement of frontier related data structures is very dynamic. Second, we identify and remove the “bubbles” in vertex status related data structures. Third, since various data structures present dynamic space requirement with respect to different sources, we propose to allocate a single memory space for all the data structures and dynamically adjust the capacity for these data structures with respect to different sources.

At a high level, we find that fill2 algorithm is similar to Dijkstra’s Single Source Shortest Path algorithm [10] in

the sense that fill2 uses the maximum vertex ID on a path to represent the “distance” metric in Dijkstra’s algorithm. The salient difference between these two algorithms lies in that one does not need to further reduce the “distance” if a fill-in is already detected in symbolic factorization. We also would like to point out that the previously proposed Δ -step optimization [39] for Dijkstra’s algorithm is not effective here: because fill2 only allows vertices that are smaller than the source to be active, Δ -step will further restrict the parallelism. However, the similarity between these two algorithms suggests that our design of multi-source, concurrent and fine-grained symbolic factorization, and out-of-core optimizations can potentially provide performance enhancement and space saving implications to multi-source Dijkstra’s algorithm.

The rest of this paper is organized as follows: Section II introduces the background of this work. Section III presents the related work and the challenges. Sections IV, V and VI present the fine-grained symbolic factorization algorithm design, concurrent multi-source symbolic factorization and space management techniques, respectively. We evaluate **gSofa** in Section VII and Section VIII draws the conclusions.

II. BACKGROUND

This section discusses the essential background for symbolic factorization including various steps of sparse LU factorization, GPU architecture and datasets specification.

A. Sparse LU Factorization

Factorizing a sparse matrix A into L and U matrices often involves several major steps, such as preprocessing, symbolic factorization and numerical factorization.

Matrix preprocessing. The matrix preprocessing performs either row (partial pivoting) or both row and column permutations (complete pivoting) in order to *reduce the number of fill-ins* in L and U matrices and *improve numerical stability* of numerical factorization. Towards the first goal, the well-known strategies encompass minimum degree algorithm [48], [43], [20], [16], [15], Reverse Cuthill-McKee [6], [21], [1] and nested dissection [28], [14], [22], [19], or a combination of them, such as METIS [27], [32], [31]. Second, numerical stability methods aim to compute a permutation to maximize the product of diagonal entries and make the matrix diagonal dominant [13], [33]. After matrix reordering, we can compute an elimination tree or a separator tree which gives the information of the independent sections in the re-ordered matrix so that later stages can take advantage of tree-based parallelism. We refer interested readers to [8] for further details.

Figure 2(a) demonstrates the matrix preprocessing on an example matrix. Particularly, we swap columns 2 and 7 so that column 2 will have 4 instead of 5 nonzeros. Further, we perform a swap between rows 2 and 3 for better numerical stability, i.e., larger numerical values are moved to diagonal.

Symbolic factorization. There mainly exist three algorithms for symbolic factorization, that is, fill1 and fill2 by Rose et al. [44] and reachability [23], [24]. They are based on the following theorem.

¹Here, out-of-core means the data is moved out of GPU memory, and stored in CPU memory.

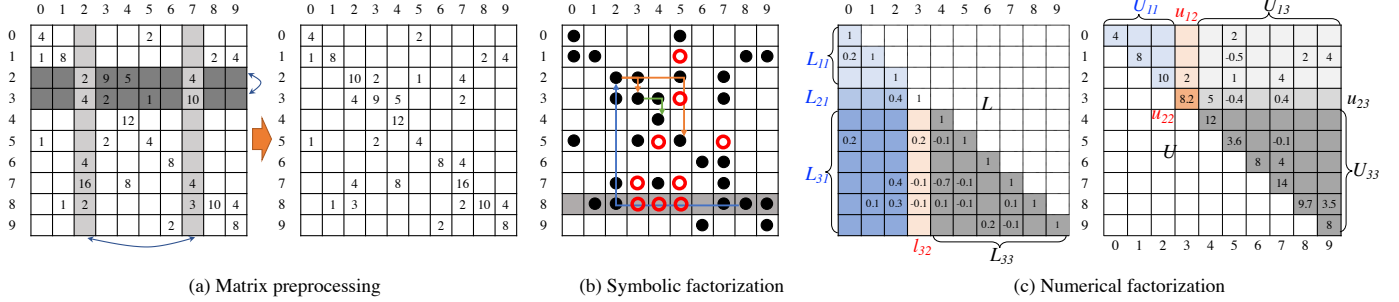


Figure 2: Major stages of LU factorization with static pivoting on a toy matrix: (a) Matrix reordering for better fill-in reduction and numerical stability, (b) Symbolic factorization and (c) Left-looking numerical factorization where assuming L_{11} , L_{21} , L_{31} and U_{11} are known blocks and l_{32} , u_{12} and u_{22} are the blocks currently being solved.

Theorem 1: A fill-in at index (i, j) is introduced if and only if there exists a directed path from i to j , with the intermediate vertices being smaller than both i and j .

Fill1 and fill2 algorithms differ in that fill1 uses $(L+U)$ while fill2 only uses A . Assuming we have already identified the fill-ins (red circles) for rows 0 - 7. At row 8, fill1 algorithm loads the neighbors of 8 and starts traversing the filled graph which includes both the original nonzeros and fill-ins. Particularly, we will find the paths $8 \rightarrow 2 \rightarrow 3$, $8 \rightarrow 2 \rightarrow 5$ and $8 \rightarrow 3 \rightarrow 4$ that satisfy Theorem 1, leading to the fill-ins $(8, 3)$, $(8, 5)$ and $(8, 4)$. Fill2 algorithm, in contrast, only works on the old matrix and finds $8 \rightarrow 2 \rightarrow 3$, $8 \rightarrow 2 \rightarrow 5$ and $8 \rightarrow 2 \rightarrow 3 \rightarrow 4$ paths that satisfy Theorem 1, which also leads to the fill-ins $(8, 3)$, $(8, 5)$ and $(8, 4)$.

In a nutshell, fill1 and fill2 can predict the structure of the potential fill-ins because they align with the elementary row operation step performed in Gaussian elimination. Particularly, Gaussian elimination contains three steps [46]. First, it puts b beside A to arrive at the augmented matrix $[A|b]$. Second, Gaussian elimination transforms A into an upper matrix through elementary row operations, that is, multiplying a row by a nonzero scalar, and adding this result to one row, leading to an updated augmented matrix $[U|b']$. Finally, triangular solver can solve $Ux = b'$ for x .

Putting Gaussian elimination in practice at row 8 of Figure 2(b), because row 8 has nonzeros at columns 1 and 2, Gaussian elimination uses the diagonal element of row 2 to eliminate the nonzero entry at $(8, 2)$. Consequently, row 2 introduce fill-ins $(8, 3)$ and $(8, 5)$ at row 8. Eventually, Gaussian elimination can use rows 3 and 5 to remove these two fill-ins, respectively. While removing the fill-in at $(8, 3)$, row 3 introduces a fill-in at $(8, 4)$.

In fact, Theorem 1 captures the two key points of this rule. First, there exists at least one path from row 8 to the fill-in. That is, since row 8 has a nonzero entry at column 2, there exists a path from vertex 8 to vertex 2 in A . Further, the nonzero columns from row 2 extends this $8 \rightarrow 2$ path to $8 \rightarrow 2 \rightarrow 3$. And further using row 3 to eliminate the fill-in $(8, 3)$ continues expand this path to $8 \rightarrow 2 \rightarrow 3 \rightarrow 4$. Second, the intermediate vertices in the path are smaller than both source and destination. Since row i in Gaussian elimination can only help remove the nonzero column i of

another row $> i$, it introduces fill-ins that are larger than i , e.g., fill-in introduced by row 2 are 3 and 5, the intermediate vertices in the path is inherently smaller than both the source and destination vertices.

A decade later, [24] introduces a different approach to finding the fill-in structures, which is in fact a simpler way of interpreting fill1 algorithm. Particularly, this approach determines the non-zero structures column by column. For clarity, we define that $L(i : j, m : n)$ and $U(i : j, m : n)$ denote the block from row i to j and column m to n in L and U matrices, respectively. For column k , it traverses the graph $L(:, 0 : k - 1)^T$ in a DFS manner, the vertex that is reachable by the vertices in column k results in a fill-in at column k . The graph used by [24] is similar to that of fill1 except that [24] applies a transpose to the L matrix. Further, whatever vertices that can be reached by [24] from the source vertices that are non-zero in $A(:, k)$, in fact, automatically satisfy Theorem 1 because [24] only uses the graph of $L(:, 0 : k - 1)^T$.

It is worth noting that the nonsymmetric-pattern sparse LU symbolic factorization is much harder than the symmetric-pattern counterpart. In the symmetric case, the transitive reduction of the filled graph $G(L)$ is a tree, called elimination tree; symbolic factorization using the elimination tree can be done in time $O(nnzeros(L))$, linear to the output size. However, for the nonsymmetric cases, the transitive reduction of the filled graphs $G(L)$ and $G(U)$ are Directed Acyclic Graphs (DAGs), called elimination DAGs. Computing these DAGs is expensive, and all variants of this method on the nonsymmetric symbolic factorization algorithms take asymptotically longer than linear time [24], [44].

Numerical factorization. Once the structure of the fill-ins is determined, the solvers perform numerical factorization to calculate the values of the L and U matrices as shown in Figure 2(c). Popular numerical factorization methods are *left-looking* [24], [9] and *right-looking* [25], [29], [11], [12], [26]. The left-looking option determines the k -th column of the filled matrix by using the computed results from columns 0 to $k-1$. Using column 3 of $(L+U)$ in Figure 2(c) as an example, we will use columns 0, 1 and 2 to solve this column. Representing A , L and U in block-matrix form, we can write LU factorization of A as follows.

Matrix (A)	Abbr.	Order (A)	nnz (A)	Struct. symm.	nnz(A) Order(A)	#Fill-in nnz(A)	Application domain
BBMAT	BB	38,744	1,771,722	0.53	45.7	18.29	Computational fluid dynamics
BCSSTK18	BC	11,948	149,090	1	12.47	6.52	Structural problem
EPB2	EP	25,228	175,027	0.67	6.93	9.28	Thermal problem
G7JAC200SC	G7	59,310	717,620	0.03	12.1	24.51	Economic modelling
LHR71C	LH	70,304	1,528,092	0	21.7	3.10	Chemical engineering
MARK3JAC140SC	MK	64,089	376,395	0.07	5.9	28.59	Economic modelling
RMA10	RM	46,835	2,329,092	1	49.729	3.14	Computational fluid dynamics
AUDIKW_1	AU	943,695	77,651,847	1	82.28	31.43	Structural problem
DIELFILTERV2REAL	DI	1,157,456	48,538,952	1	41.93	22.39	Electromagnetics problem
G3_CIRCUIT	G3	1,585,478	7,660,826	1	4.83	24.02	Circuit simulation
HAMRLE3	HM	1,447,360	5,514,242	0	3.8	32.63	Circuit simulation
PRE2	PR	659,033	5,834,044	0.33	8.8	20.70	Circuit simulation
STOMACH	ST	213,360	3,021,648	0.85	14.2	25.77	Bioengineering
TWOTONE	TT	120,750	1,206,265	0.24	10	6.07	Circuit simulation

Table I: Dataset specifications. Note, in graph terminology, order (A) and nnz(A) represent $|V|$ and $|E|$ of the graph $G(A)$, respectively, where A is the matrix of interest.

$$\begin{bmatrix} L_{11} & & \\ l_{21} & 1 & \\ L_{31} & l_{32} & L_{33} \end{bmatrix} \begin{bmatrix} U_{11} & u_{12} & U_{13} \\ & u_{22} & u_{23} \\ & & U_{33} \end{bmatrix} = \begin{bmatrix} A_{11} & a_{12} & A_{13} \\ a_{21} & a_{22} & a_{23} \\ A_{31} & a_{32} & A_{33} \end{bmatrix}, \quad (1)$$

where $L_{11} = L(0 : 2, 0 : 2)$, $l_{21} = L(3 : 3, 0 : 2)$, $L_{31} = L(4 : 9, 0 : 2)$, $l_{32} = L(4 : 9, 3 : 3)$, $L_{33} = L(4 : 9, 4 : 9)$, $U_{11} = U(0 : 2, 0 : 2)$, $u_{12} = U(0 : 2, 3 : 3)$, $U_{13} = U(0 : 2, 3 : 9)$, $u_{22} = U(3 : 3, 3 : 3)$, $u_{23} = U(3 : 3, 4 : 9)$, and $U_{33} = U(4 : 9, 4 : 9)$. The texts in green, red and black colors represent the known, currently under solving, and unknown blocks, respectively. Through block matrix multiplication of Equation (1) towards a_{12} , a_{22} and a_{32} , we further obtain:

$$\begin{aligned} L_{11}u_{12} &= a_{12}, \\ l_{21}u_{12} + u_{22} &= a_{22}, \\ L_{31}u_{12} + l_{32}u_{22} &= a_{32}, \end{aligned} \quad (2)$$

where u_{12} , u_{22} and l_{32} are computed in order in Equation (2) so that the u_{22} and l_{32} can be calculated once u_{12} is resolved in the first equation of Equation (2).

B. General Purpose GPUs

This section discusses general purpose GPUs, particularly the streaming processor, memory architecture and fine-grained parallelism. Particularly, we use recent NVIDIA V100 GPU [40] to describe the details.

Streaming processors and threads. The V100 GPU is designed with NVIDIA Volta architecture. V100 is powered by 80 Streaming Multiprocessors (SMX). Each SMX features 64 CUDA cores resulting in a total of 5,120 CUDA cores. During execution, a GPU thread runs on one CUDA core. A SMX schedules a group of 32 consecutive threads known as warp in a SIMT manner. A collection of consecutive warps further formulate a Cooperative Thread Array (CTA), or a block. All the CTAs together in one kernel are called a grid.

Memory architecture. V100 comes with two memory capacities, that is, 16 GB and 32 GB with peak bandwidth up to 900 GB/s. Each SMX has 96 KB on-chip fast memory that is shared by configurable shared memory and L1 cache.

All the SMXs share a L2 cache at size of 6,144 KB. Each thread block can use up to 65,536 32-bit registers.

Fine-grained parallelism. It is important to note that GPUs favor fine-grained parallelism. Particularly, GPUs can only achieve the aforementioned ideal computing and memory throughput when a warp of threads is working on the same instruction and fetching data from consecutive memory addresses. Otherwise, GPUs might suffer from either warp divergence or uncoalesced memory access issues, resulting in an order of magnitude performance degradation [40].

C. Dataset

Table I presents the datasets, all of which are available from Suite Sparse Matrix Collection [4] to evaluate GSOFA. Particularly, the matrices include applications from circuit simulation (G3, HM, PR, and TT), structural problems (BC, AU), computational fluid dynamics (BB and RM), thermal problems (EP), economic modelling (G7 and MK), chemical engineering (LH), electromagnetics problem (DI) and bioengineering (ST). Same as SuperLU_DIST, we use ParMETIS [30] library to reorder the matrix for fill-in reduction. With this ordering, the ratio of fill-in to that of original non-zeros in the matrix varies in the range of 3.10 to 32.63 in the test datasets. Besides, this dataset collection covers a wide range of variations in both structural symmetry and sparsity (the last two columns in Table I). This table arranges the datasets into smaller (upper) and larger (lower) collections with respect to order (A). And the larger matrices are used in space complexity analysis in Section VII. Following SuperLU_DIST, we adopt Compressed Sparse Row (CSR) format to represent the matrices [35], [38].

III. RELATED WORK AND DESIGN CHALLENGES

This section studies the recent advances in symbolic factorization and summarizes the design challenges faced by scaling symbolic factorization towards a large number of GPUs.

Challenge #1. Existing symbolic factorization algorithms present limited fine-grained parallelism.

Fill2 algorithm [44], as shown in Figure 4(a), uses fill[] to indicate an already visited vertex by setting the corresponding

entry to be src . That is, $fill[v]=w$ means that vertex v is visited in the traversal when w is a source. For the vertices that are not yet visited in the current traversal starting with source src , their values of $fill[]$ remain smaller than src . During traversal, this algorithm only permits traversing one vertex (i.e., threshold) at a time, starting from the smallest one (line 6 - 7). For each threshold which is treated as a frontier, this algorithm checks its neighbors, updates the statuses of the neighbors in $fill[]$ array, and adds new fills to the filled graph $G(F)$, as well as to the $newfrontierQueue[]$ if this neighbor obeys Theorem 1 (line 15). This process continues until the vertices that are smaller and connected to the threshold vertex are exhausted, i.e. $frontierQueue[]$ is empty. Subsequently, $fill2$ will proceed to the next threshold vertex in line 6.

The major problem of $fill2$ is that line 6 - 7 only allows processing one threshold vertex at a time. It is important to note that *simply allowing fill2 to process multiple threshold vertices in parallel will not warrant correctness* because the threshold value has to be strictly increased sequentially. The core reason lies in the constraint that each vertex can only be visited once in $fill2$. We demonstrate this fact by the detection of the fill-in $(8, 4)$ from Figure 5. At line 4 in $fill2$ algorithm, the $fill[]$ of all the neighbors of source 8, that is, $\{1, 2, 7\}$, will be 8. Assuming multiple threads can work in parallel at line 6, implying the thresholds will be 1, 2 and 7 from three different threads, respectively. In that case, all the neighbors 1, 2 and 7 will be inserted into the $frontierQueue[]$. When accessing the neighbor of the frontier at line 9, if a thread working on frontier 7 explores vertex 4 before any other threads, $fill2$ will update $fill[4] = 8$ without a fill at $(8, 4)$ because the path $8 \rightarrow 7 \rightarrow 4$ does not satisfy Theorem 1. Later, the thread that could introduce a fill at $(8, 4)$ because of path $8 \rightarrow 2 \rightarrow 3 \rightarrow 4$ will fail to do so because this thread will fail to enter the branch at line 9 since $fill[4] = 8$. Hence, the fill-in $(8, 4)$ remains undetected.

Instead of processing the frontier vertices with minimum threshold in $fill2$ [44], we allow all frontiers to be processed in parallel, such that the adjacent GPU threads can work on similar tasks. *Given this relaxation might work on some frontiers earlier than they are supposed to, we introduce data structures and control logic to allow re-visitations in order to ensure the correctness which is the key of this technique.*

Challenge #2. Various sources exhibit imbalanced workload.

Theorem 1 suggests two important implications. First, the amount of workload per source generally increases with respect to the ID of the source because potentially more intermediate vertices will be smaller than the source when the source is larger. Our experimental results in Figure 3 also align with this fact. The rough trend is that the workload soars with the rise of the source IDs. For instance, the workload differences between the smallest and largest sources are $1,265\times$, $167\times$, $6,230\times$, $49,726\times$ for BC, RM, TT and PR datasets, respectively. Second, the workload of the small sources might not be able to saturate a single GPU.

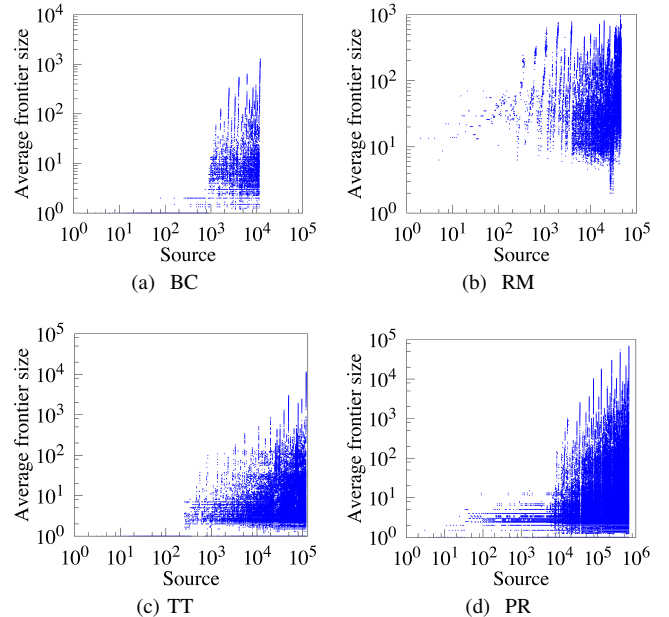


Figure 3: Average frontier size per source of different datasets. Note, we only present BC, RM, TT and PR for the sake of space, as well as including both small and large datasets.

This workload dynamic leads to a workload imbalance problem for both inter- and intra- GPUs. Towards the first issue, we introduce an interleaved source scheduling among GPUs. In particular, the interleaved source scheduling help avoid inter-GPU workload imbalance. Further, we combine all the sources that are assigned to a single GPU during traversal so that the workloads emitted by all sources are shared by all GPU threads, leading to a balanced workload distribution.

Challenge #3. Multi-source concurrent symbolic factorization consumes overwhelming memory space.

While runtime is important for symbolic factorization, so is space consumption. For instance, symbolic factorization is merely a step of LU decomposition which is further only a component for some memory hungry applications, such as, circuit simulation [2] and computational fluid dynamics [42]. Consequently, it is important to reduce the memory usage of symbolic factorization. However, for each source, GSOFA needs six nontrivial data structures, each of which will consume memory space at size of $\mathcal{O}(|V|)$. Further, since we often need tens to thousands concurrent sources in order to saturate a GPU (discussed in Section V), the ideal space consumption for certain matrices becomes significantly larger than the available memory space on GPUs.

This paper introduces the following space management strategies: First, we stream all the newly detected fill-ins off of the GPU on the fly. Second, we treat various data structures differently. For the sequentially accessed ones, we introduce out-of-core management. Third, we identify and put the bubbles from allocated space into good use. Last but not the least, we allocate a gigantic array to serve the dynamic

```

1: Input: fill[], src, adj, frontierQueue[], newFrontierQueue[]
2: Output: G(F) of row src
3: Initialization: fill[] = 0; //Only once
4: fill[src] = src;
5: forall v in adj(src) fill[v] = src;
6: for threshold = 0 to src -1 s.t. fill [threshold] == src do
7:   add threshold to frontierQueue[];
8:   forall frontier  $\in$  frontierQueue[] do
9:     forall neighbor  $\in$  adj (frontier) do
10:      if fill [neighbor] < src
11:        fill [neighbor] = src;
12:        if neighbor > threshold
13:          add (src, neighbor) to G(F);
14:        else //if neighbor  $\leq$  threshold
15:          add neighbor to newFrontierQueue[];
16:   swap (frontierQueue[], newFrontierQueue[]);

```

(a) Fill2 algorithm

```

1: Input: maxId[], src, adj, frontierQueue[], newFrontierQueue[]
2: Output: G(F) of row src
3: Initialization: maxId [] = maxVal; //Initialize every  $\frac{\text{maxVal}}{|V|}$  number of src
4: maxId [src] = 0;
5: forall v in adj (src) fill[v] = 0, maxId [v] = 0, add (src, v) to G(F);
6: forall v in adj (src) such that v < src, add src to frontierQueue[];
7: forall frontier  $\in$  frontierQueue[] in parallel do //Fine-grained parallelism
8:   newMaxId = Max (frontier, maxId [frontier]);
9:   forall neighbor  $\in$  adj (frontier) in parallel do //Fine-grained parallelism
10:    if atomicMin(maxId[neighbor], newMaxId) > newMaxId do
11:      if neighbor > newMaxId do
12:        if (atomicMax (fill[neighbor], src) < src)
13:          //if not detected as fill-in before
14:          add (src, neighbor) to G(F);
15:        else continue; //Avoid re-insertion to frontierQueue[]
16:   swap (frontierQueue[], newFrontierQueue[]);

```

Line 9.5
if fill[neighbor] == src **continue;**
//Enable line 9.5 when
there exists large number of
fill in the graph.

(b) GSOFA algorithm

Figure 4: Algorithms: (a) Fill2 algorithm [44], (b) GSOFA parallel algorithm.

needs of different sources to both maximize the performance and allow configurable space consumption for GSOFA.

IV. FINE-GRAINED PARALLEL SYMBOLIC FACTORIZATION ALGORITHM

GSOFA addresses the aforementioned challenges faced by fill2 by 1) allowing parallel processing of the frontiers with 2) adding a new data structure maxId[] of size $|V|$, and 3) a new logic to allow revisit. Below we explain the data structure and algorithm design separately. Formally, from the source vertex src to a specific vertex v , there often exist multiple paths, and each path has a maximum numbered vertex. maxId[v] stores the minimum of all the maximums of the paths from src to v .

GSOFA allows repeated update to maxId[] along the traversal. And the traversal terminates once the maxId values of all the vertices converge to their minimal value. As shown in Figure 4(b), at the beginning, the neighbors of src that are smaller than src are qualified for continuing traversal along these neighbors. Hence they are inserted into frontierQueue[] at line 6. During traversal, the algorithm allows all the frontiers to explore the graph in parallel. With initial setting of 0 for every vertex, fill[v] of a vertex v in the algorithm is set to src if there is a nonzero (src, v) in the filled graph. The value of fill[] helps avoid re-detection of fill-ins at line 12. For a vertex v , fill[v] $<$ src means that vertex v is not yet in the filled structures of row src in the matrix.

GSOFA fulfills two tasks in lines 9 - 15. The first task is to check whether a neighbor will introduce a fill. The second task is to decide whether a vertex can become a frontier? For both tasks, we need the new path from the frontier to the current neighbor to change the maxId of this neighbor, that is, maxId[neighbor] should be updated by newMaxId at line 8. Further, for the first task, this neighbor needs to satisfy Theorem 1. And this neighbor should have not introduced a fill before, i.e., line 12. Otherwise, we face the issue of re-insertion of this neighbor into G(F). For the second task, a neighbor needs to meet three criteria in order to become frontier, that is, this neighbor is smaller than the source, has an update to maxId (line 10) and has not introduced a fill yet (line 12).

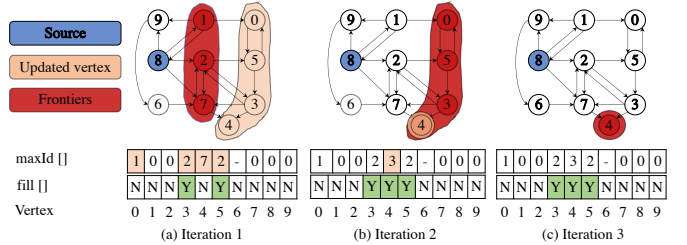


Figure 5: GSOFA traversing the graph that is identical to the matrix in Figure 2(a). The blue, dark brown, and orange vertices respectively represent the source, current frontier, and updated vertices. The maxId[] and fill[] are at size of $|V|$.

Otherwise, this neighbor either cannot be a frontier or has already been enqueued in the newFrontierQueue[].

Example. To aid the understanding of GSOFA, Figure 5 demonstrates how GSOFA traverses from $src = 8$ on the graph that is identical from the matrix of Figure 2(b). After line 5, the values of the vertices $\{1, 2, 7, 8, 9\}$ in maxId[] array become 0, while the rest remain as $|V|$ (i.e., ‘-’ in this case).

At iteration 1, the frontiers $\{1, 2, 7\}$ will, in parallel, traverse their neighbors $\{0, 8, 9\}$, $\{3, 5, 7\}$ and $\{2, 4\}$, arriving at updated maxId[] and fill[] array at the bottom of Figure 5(a). Particularly, we will obtain 1, 2, 7 and 2 as the maxId along the path $8 \rightarrow 1 \rightarrow 0$, $8 \rightarrow 2 \rightarrow 3$, $8 \rightarrow 7 \rightarrow 4$ and $8 \rightarrow 2 \rightarrow 5$. Clearly, these paths introduce the fill at 3 and 5 as shown in the fill[]. Proceeding to iteration 2, frontiers $\{0, 3, 4, 5\}$ will generate new paths as $8 \rightarrow 1 \rightarrow 0 \rightarrow 5$, $8 \rightarrow 2 \rightarrow 3 \rightarrow 4$ and $8 \rightarrow 2 \rightarrow 5 \rightarrow 3$. Even $8 \rightarrow 1 \rightarrow 0 \rightarrow 5$ will update maxId[5] at line 10, it will not introduce a fill due to line 12, thus 5 will not be enqueued into newFrontierQueue[]. Path $8 \rightarrow 2 \rightarrow 5 \rightarrow 3$ will stop at line 10 because the stored maxId[3] = 2 is smaller than the newMaxId = 5. Finally, path $8 \rightarrow 2 \rightarrow 3 \rightarrow 4$ will qualify line 10 since the stored maxId[4] = 7 which is greater than newMaxId=3, as well as introduce a new fill due to line 12 is true. Afterwards, only 4 is in the newfrontierQueue[] at iteration 3 which will not introduce any new frontiers.

Optimizing the initialization of maxId[]. Maintaining a maxId[] array for every traversal would require excessive

amount of space that becomes impractical for large datasets considering limited memory space on modern GPUs. Hence reusing `maxId[]` array for different sources becomes essential. But this reusage also comes with re-initialization overhead, that is, making `maxId[]` to `maxVal` before traversal. And this overhead is nontrivial, e.g., it takes 22% of the total time for PR dataset to re-initialize the `maxId[]`.

To reduce the re-initialization overhead, we propose to divide the value range $[0, maxVal]$ of `maxId[]` into smaller ranges, i.e., $[0, |V|]$ for multiple sources, i.e., `maxVal` is 2^{32} for an integer type. During traversal, different sources can work on their respective value range of `maxId[]` without re-initialization. For instance, for the first source, the traversal updates the `maxId` of the vertices in the range of $[maxVal - |V|, maxVal]$. Moving to the next source, we regard the range of $[maxVal - 2 \cdot |V|, maxVal - |V|]$ as valid for `maxId`. In this context, any `maxId` value that is out of this range is treated as initialized. This optimization helps skip the `maxId[]` initialization for a total of $\frac{maxVal}{|V|}$ sources. For instance, it helps reduce the re-initialization cost of PR dataset from 22% to 0.082% of the total time.

Optimizing the access to `maxId[]` and `fill[]`. It is important to mention that the accesses to both `maxId[]` and `fill[]` array are random thus time consuming. One can either access `maxId[]` first to reduce the follow-up access to `fill[]` or vice versa (i.e., adding line 9.5 to the pseudo code). In both cases, we avoid repeated frontier enqueueing for vertices that are already detected as fill-ins at line 14.

Putting `maxId[]` access before `fill[]`, which is the pseudo code in Figure 4(b), will avoid the access to `fill[]` array when the new path fails to update the `maxId` of existing paths, i.e., line 10 is evaluated as false. Consequently, this path avoids the access to follow-up `fill[]` at line 12. Path $8 \rightarrow 7 \rightarrow 4$ from Figure 5(a) falls in this case.

Adding line 9.5 to the pseudo code in Figure 4(b) will avoid unnecessarily lowering the `maxId` of an already detected fill-in. Note, we do not need to do so because this vertex will always propose its own vertex ID as the `maxId[]` for the paths that come across this vertex. Using Figure 5(a) as an example, this logic avoids lowering `maxId[5]` from 2 to 1 when the path $8 \rightarrow 1 \rightarrow 0 \rightarrow 5$ attempts to do so because $(8, 5)$ is already a fill due to $8 \rightarrow 2 \rightarrow 5$. And the continuation of the paths from 8 through 5 will surely use 5 as the `maxId`.

Including line 9.5 or not is a graph dependent option. Particularly, adding line 9.5 is beneficial for graphs which have relatively larger number of fill-ins. But for graphs with relatively smaller number of fill-ins, the condition of line 9.5 will become false for most of the time, resulting in higher overhead than benefits.

V. MULTI-SOURCE CONCURRENT SYMBOLIC FACTORIZATION

Multi-source concurrent symbolic factorization, which executes multiple sources of the Algorithm in Figure 4(b) concurrently on a single GPU, is essential for fast symbolic factorization stemming from two facts. First, we need each

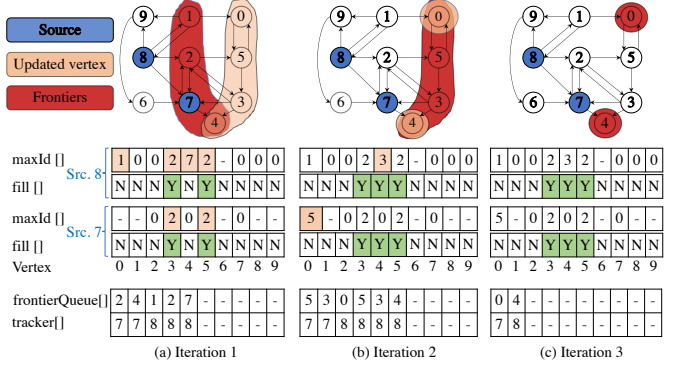


Figure 6: GSOFA’s combined traversal with vertices 7 and 8 as sources of traversal. `frontierQueue[]` and `tracker[]` are the combined `frontierQueue[]` and `tracker[]` for the two sources.

GPU to handle multiple sources. While GSOFA exhibits fine-grained parallelism that is well suited for modern GPUs, one cannot afford $|V|$ number of GPUs for symbolic factorization. This leads to the fact that each GPU should account for more than one source. Second, each source cannot fully saturate a single GPU. As shown in Figure 3, certain sources only come with tens of frontiers which obviously cannot saturate a GPU. So instead of one GPU processing a single source at a time, we can work on several sources concurrently.

Warp-centric GSOFA. This work studies both thread- and warp- centric designs, where thread-centric assigns a thread to a frontier while warp-centric assigns a warp. We find thread-centric performs better for smaller datasets or the datasets with smaller $\frac{nnz(A)}{n}$, i.e., BC, EP, HM and G3 with fewer GPUs and warp-centric bests for the rest. The reason is that each frontier does not have enough workload to fully saturate a warp in those datasets.

A naive version of the multi-source concurrent symbolic factorization would evenly partition the threads of one GPU to each source. Subsequently, all sources can be executed concurrently for fill-in detection. However, *as discussed by Challenge #2 of Section III, the workload of various sources vary by orders of magnitude*. Hence, the naive design will experience two types of workload imbalance, that is, intra- and inter- GPU workload imbalance.

Combined traversal for intra-GPU workload imbalance. To ultimately balance the workload across all GPU threads, we propose to combine the workloads of all the concurrently executed sources on the same GPU. Combined symbolic factorization in GSOFA comes with two key features 1) the combined frontier queue, and 2) each warp on the GPU is assigned to a frontier irrespective to the source of traversal. As we merge the frontiers of different traversals into the same frontier queue, we also need to track which source each frontier comes from in order to determine the correct fill-structure. We hence introduce a `tracker[]` array which is at the same size as `frontierQueue[]` to indicate the sources of each frontier. During traversal, each GPU warp can dynamically fetch the next frontier that is currently available in the `frontierQueue[]` through `atomicAdd` [18].

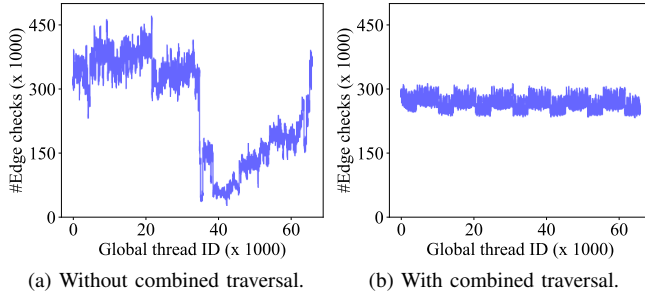


Figure 7: #Edge checks before and after combined traversal optimization on PR dataset.

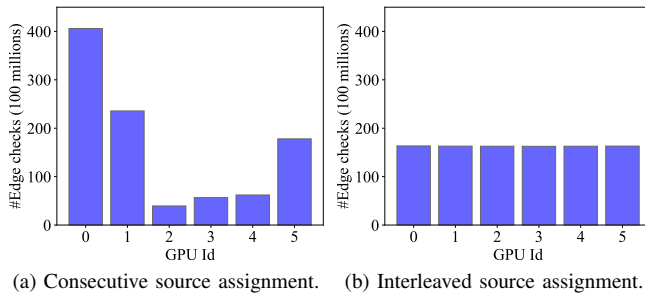


Figure 8: Before and after inter-GPU workload balancing optimization on PR on one summit node.

Figure 6 demonstrates an example of combined traversal with two concurrent sources, i.e., 7 and 8). Sources 7 and 8 are assigned source indices of 0 and 1, respectively. At iteration 1, the `frontierQueue[]` is initialized with the neighbors of sources (such that $\text{neighbor} < \text{source}$), i.e., $\{2, 4, 1, 2, 7\}$, and their corresponding source ID in `tracker[]`. At iteration 2, the frontier 2 of source 7 introduces frontiers $\{3, 5\}$ while frontiers $\{1, 2, 7\}$ of source 8 introduce frontiers $\{0, 5, 3, 4\}$. At iteration 3, source 7 has the frontier 0 whereas source 8 introduces frontier 4 through the frontier 3.

Figure 7 demonstrates the #edge checks per thread in a GPU before and after the optimization of the combined traversal. Clearly, the workload per thread becomes closer to each others after the optimization. Particularly, the ratio of maximum and minimum #edge checks before and after combined traversal are 45.78 and 1.34, respectively.

Inter-GPU workload imbalance. While intra-GPU workload imbalance is ultimately resolved by combined symbolic factorization, inter-GPU workload imbalance remains problematic if we assign a consecutive number of sources to a GPU. The reason lies in the nature of Theorem 1. Particularly, the amount of workload climbs from small to large sources because this theorem only allows vertices that are smaller than the source to be frontiers. This is evident both through the algorithm and evaluation. First, in GSOFA of Figure 4(b), we only enqueue vertices that are smaller than source at lines 6 and 15. Second, revisiting Figure 3, we observe that the trend of average frontier size per source increases.

We introduce interleaved source assignment to combat the inter-GPU workload imbalance. This strategy is implemented in GSOFA’s multi-GPU version where the sources are assigned to each GPU in a round-robin fashion. For instance, assuming

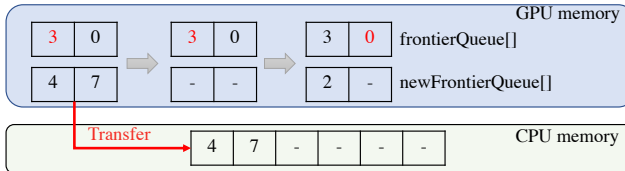
using two GPUs to process a graph of four vertices, we will assign sources $\{0, 2\}$ to GPU 0 and $\{1, 3\}$ to GPU 1. Such a round-robin assignment of sources helps avoid the inter-GPU workload imbalance problem in multi-GPU configuration. It is important to mention that *even with interleaved source assignment, this work still supports supernode detection (with $< 1\%$ overhead) which is crucial for the downstream numerical factorization*. Figure 8 demonstrates the impacts of interleaved source assignment. As it can be observed that the #edge checks per GPU becomes more balanced after the optimization. Particularly, the ratio of maximum and minimum #edge checks is reduced from 10.31 to 1.01 after interleaved source assignment.

Distinction from the previous work. It is important to note that GSOFA’s multi-source concurrent symbolic factorization is inspired by the recent work [47], [36]. However, our contribution is fundamentally different from them in two ways. First, symbolic factorization experiences drastically different workload from various sources, making workload imbalance the major concern. In contrast, various sources of multi-source Breadth-First Search (BFS) experience similar workload and mainly concern about irregular memory access to algorithmic metadata [47], [36], [49]. Therefore, GroupBy optimizations from iBFS [36] is actually harmful to symbolic factorization. Second, symbolic factorization requires an update to the `maxId` with the minimum of the maximum among all the paths from the source to the current vertex. This is different from BFS which only concerns about either visited or not. Therefore, the bitwise optimizations from MS-BFS [47] and iBFS [36] are not applicable for symbolic factorization. In summary, GSOFA contributes to workload balancing while the prior work optimizes memory access.

VI. SPACE COMPLEXITY AND OPTIMIZATION

Continuing our discussion in Challenge #3 of Section III, this section will rigorously quantify the *space crisis faced by multi-source concurrent symbolic factorization*. Table II presents the space complexity of the six major data structures used by GSOFA, namely, `frontierQueue[]` & `newFrontierQueue[]`, `tracker[]` & `newTracker[]`, `maxId[]`, and `fill[]`. When the number of concurrent sources is $\#C$, the total space consumption would be around $6 \cdot |V| \cdot \#C$ entries. Apparently, space consumption immediately becomes a key problem for large graphs with relatively big number of concurrent sources. Using PR graph as an example, as we will show shortly in Figure 12, the performance keeps climbing with respect to the rise of $\#C$ to 1,024. There is a chance of further improving the performance if we can make $\#C$ bigger. But we will need ~ 30.16 GB of memory to support the execution of $\#C = 2,048$ sources which ultimately goes beyond the available memory space of V100 GPUs on Summit [41].

In this section, we propose three interesting optimizations based upon the access pattern and usage of various data structures to combat the high space complexity. Particularly, we introduce out-of-core frontier management, bubble removal in `maxId[]`, dynamic space allocation to dynamically assign



(a) Using CPU memory as the buffer for out-of-core frontier management.

Figure 9: Space complexity optimizations using out-of-core frontier management.

Data structure	Space complexity
frontierQueue[] & newFrontierQueue[]	$2 \cdot V \cdot \#C$
tracker[] & newTracker[]	$2 \cdot V \cdot \#C$
maxId[]	$ V \cdot \#C$
fill[]	$ V \cdot \#C$

Table II: The data structures used by multi-source concurrent GSOfA, where $|V|$ and $\#C$ are the number of vertices in the graph, and concurrent sources, respectively.

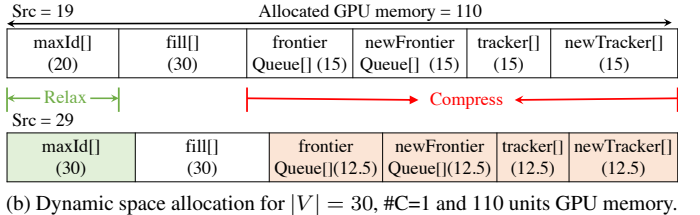
Dataset	Average usage (%)	Peak usage (%)
AU	0.12	8.2
DI	0.04	4.55
G3	0.1	1.0
HM	0.01	1.7
PR	0.11	25.0
ST	0.1	1.0
TT	0.1	11.0

Table III: Percentage of usage of allocated frontier queues for different datasets.

memory space to various data structures. Note, this dynamic space allocation also allows GSOfA to support configurable space consumption.

Out-of-core frontier management is motivated by the observation in Table III where the average usage of frontier related data structures remains low for the large datasets, i.e., AU, DI, G3, HM, ST and TT. However, the peak usage can rise to as high as 25% for PR. This observation implies that we can allocate relatively smaller memory space to hold frontier related data structures because the usage remains low for vast majority of the iterations. Once the peak usage becomes large, we can deal with it through out-of-core option.

We propose to only allocate a fraction of the required space on GPU for the four frontier related data structures, i.e., frontierQueue[], newFrontierQueue[], tracker[] and newTracker[] and write the extra frontiers out-of-GPU. During computation, we load these out-of-GPU data structure in GPU for computation. Figure 9(a) demonstrates this design. For brevity, Figure 9(a) only uses a single thread to traverse the graph for source 5 without loss of generality. The size of the allocated newFrontierQueue[] is only two. At iteration 1, frontier 3 exhausts the newFrontierQueue[] by its neighbors 4 and 7. Subsequently, we copy these two frontiers to CPU memory so that we still have available space for the incoming frontiers, 2 in this case. Proceeding to next iteration that comes after swapping the queues, we will finish frontier 2 in the frontierQueue[] first and load the frontiers from CPU memory in GPU for further computation. It is worthy of mentioning that, instead of directly storing the source ID in tracker[] and newTracker[] in Figure 6, we propose to store the index of the



(b) Dynamic space allocation for $|V| = 30$, $\#C=1$ and 110 units GPU memory.

source for each frontier. Hence we can use fewer bits for the tracker[] and newTracker[].

Bubble removal in maxId[] is supported by the key observation that a source vertex is not allowed to traverse beyond vertices that are larger than the source. Consequently, we can remove the “bubbles” in the maxId[] that are larger than the source. Here, “bubble” means the allocated space that is not used in maxId[]. Assuming the source vertex is v , according to Theorem 1, we will never update the maxId of the vertices that are larger than v . Consequently, we do not need entries for those larger vertices.

Dynamic space allocation across data structures is motivated by two facts. First, maxId[] and fill[] accesses are more random than frontier-related data structure. Particularly, the accesses to maxId[] and fill[] are determined by the neighbors of each frontier. Since a vertex often connects to random neighbors, the accesses to maxId[] and fill[] are hence random. In contrast, the accesses to frontiers in frontierQueue[] are sequential and consecutive. Second, the space requirement for maxId[] increases with respect to the source index. For instance, larger sources need more maxId[] space. Therefore, it is natural to dynamically adjust the spaces for various sources.

Towards this end, we first allocate a big chunk memory, in contrast to allocating separate memory spaces for various data structures discussed in Table II. Subsequently, this memory chunk is dynamically divided among the data structures with priority given to maxId[] and fill[]. For a given number of concurrent sources in a traversal, after the space reduction strategy of maxId[], the amount of memory required for maxId[] remains low for the large graph. In this scenario, we can allocate more space for other data structures. Once we start to work on larger sources, the maxId[] space requirements begin to climb. In this context, we prioritize the space requirement for maxId[] along with fill[] so that a large number of concurrent sources can execute together with roughly sustained performance.

Figure 9(b) demonstrates the dynamic memory allocation. Considering a graph with $|V| = 30$, the allocated amount of GPU memory allocated = 110 units and $\#C = 1$ for explanation simplicity. Assuming the source ID is 19, maxId[] requires 20 units of GPU memory. With 30 units required for fill[], we can afford 60 units for the remaining four major data structures.

When the source becomes 29, maxId[] requires 30 units of GPU memory. In this case, we will allow 50 units for the remaining data structures.

GSOfA with space configurability. After putting all the

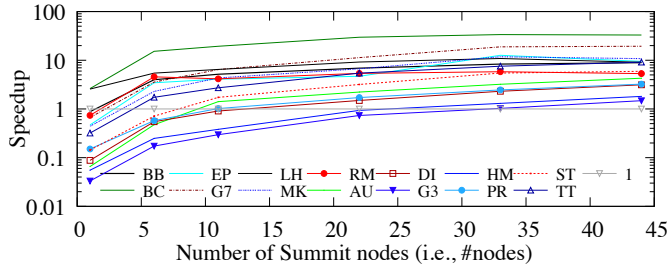


Figure 10: Speedup of GSOFA over the CPU parallel symbolic algorithm in SuperLU_DIST.

major data structures of GSOFA into a gigantic memory space, we further enable GSOFA to execute in any configured memory budget. This optimization will first conduct bubble removal and out-of-core frontier related data structure management. If GSOFA still suffers from space shortage, GSOFA will automatically reduce the number of concurrent sources in order to restrict GSOFA’s memory space consumption into this given envelop.

VII. EVALUATION

We implement GSOFA with $\sim 2,500$ lines of C++/CUDA code. The code is compiled by NVIDIA CUDA 10.1 Toolkit with the optimization flag set to be O3. For scalability test, we resort to IBM Spectrum MPI 10.3.0.0, where each MPI process manages one V100 GPU. We study GSOFA on the Summit supercomputer at Oak Ridge National Laboratory [41], where each computing node is equipped with dual-socket IBM POWER9 CPU processors (i.e., 44 cores), and six NVIDIA Volta GPUs. All the GPUs on one Summit node are connected with NVIDIA’s high-speed NVLink.

Comparison with a state-of-the-art CPU algorithm.

Figure 10 demonstrates the performance comparison between GSOFA and the CPU parallel symbolic factorization in SuperLU_DIST.

As expected, GSOFA starts worse than the CPU parallel algorithm for majority of the datasets. However, with more and more Summit nodes, GSOFA begins to outperform the CPU algorithm on more and more datasets. Particularly, initially on one node, GSOFA is 2.6 \times and 2.6 \times faster on BC and LH, respectively and 1.1 \times , 2.1 \times , 1.5 \times , 2.3 \times , 1.4 \times , 15.2 \times , 30.1 \times , 18.1 \times , 6.6 \times , 6.9 \times and 3.1 \times slower on BB, EP, G7, MK, RM, AU, DI, G3, HM, PR, ST and TT, respectively on one node. When it goes to six Summit nodes, GSOFA bests CPU parallel symbolic factorization on majority of the datasets, i.e., BC, EP, BB, RM, G7, MK, LH and TT. GSOFA finally beats CPU parallel symbolic factorization across all the datasets when scaling to 44 Summit nodes, at which the maximum speed-up of 32 \times is achieved for BC matrix and minimum of 1.48 \times is achieved for G3 matrix.

Performance impact of workload balancing techniques.

Figure 11 examines the performance impacts of different optimization techniques to balance workload. Note, we use six nodes (i.e., 36 GPUs) in order to showcase the impacts of our inter-GPU workload balancing strategies. Specifically, the

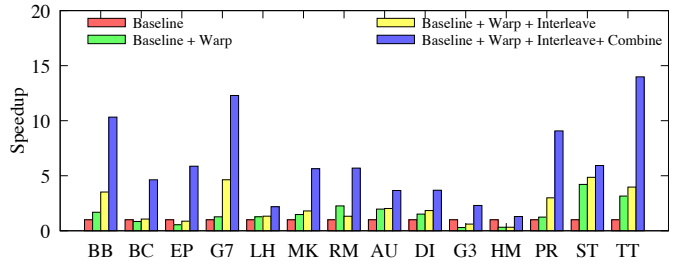


Figure 11: Performance impacts of different workload balancing optimizations on six nodes (i.e., 36 GPUs).

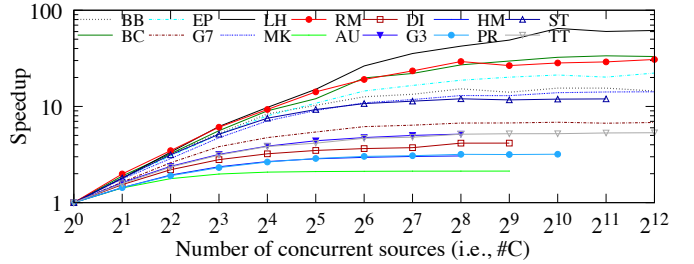


Figure 12: Speedup of combined traversal over #C=1 on different dataset. #C is varied from 1 to 4,096.

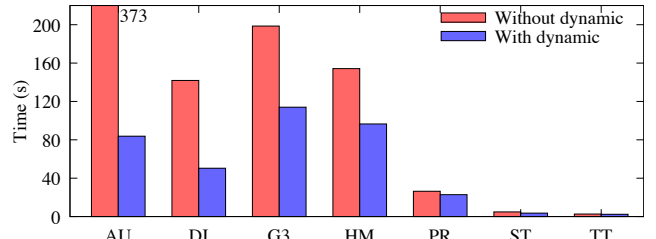


Figure 13: Performance impacts of dynamic space allocation on one GPU.

“baseline” version assigns one CTA to each source with a single thread working on one frontier. The “warp”-centric assigns one warp to each frontier. “Combine” puts all sources together and “interleave” deals with inter-GPU source assignment. As shown in Figure 11, warp-centric achieves, on average, 1.45 \times speedup over baseline. Interleave adds another 2.23 \times speedup over warp-centric with combine further yielding, on average, 6.18 \times speedup. The maximum gains of warp-centric, interleave and combined are 4.21 \times (ST), 4.85 \times (ST) 13.96 \times (TT), respectively.

Performance impact of different number of concurrent sources (i.e., #C). As shown in Figure 12, the general trend is that the overall performance climbs as #C soars. Further, the benefits of combined traversal is more pronounced for smaller datasets like BC, EP and RM while larger datasets like AU, DI, PR and HM tend to provide large enough workload to saturate the GPUs with relatively smaller #C. For small datasets, e.g., BB, BC, EP, G7, LH, MK and RM, we get the maximum speedup of 14.47 \times , 33.03 \times , 22.23 \times , 6.81 \times , 61.63 \times , 14.20 \times , 30.77 \times , respectively. For larger datasets, e.g., AU, DI, G3, HM, PR, ST and TT we observe maximum speedup of 2.12 \times , 3.73 \times , 5.16 \times , 3.06 \times , 3.18 \times , 11.91 \times and 5.30 \times , respectively.

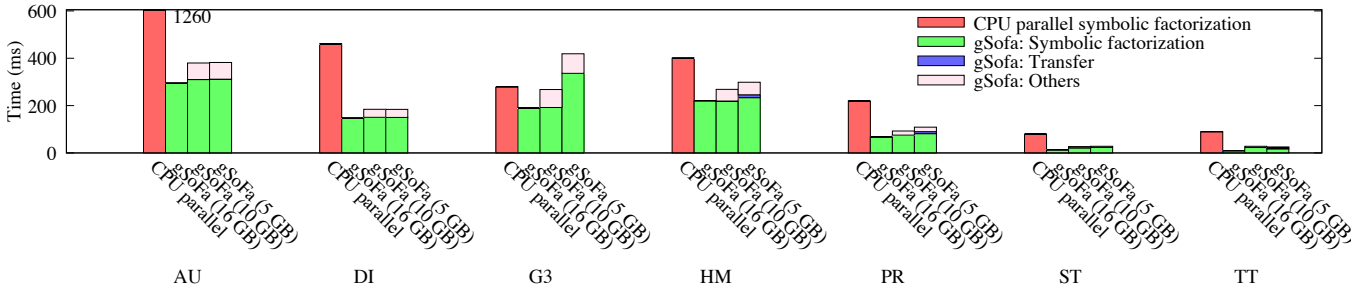


Figure 14: Performance study of gSOFA at different memory allocations compared to CPU parallel symbolic factorization from SuperLU_DIST on 44 summit nodes. The amount of GPU memory allowed for all the data structures in gSOFA is varied from 16 to 5 GB.

Impact of dynamic space allocation. Figure 13 presents the effect of dynamic memory allocation. We allocate 1 GB of memory and evaluate the performance of the codes with and without the dynamic memory optimization. As expected, this optimization yields performance gains for all large datasets in Table I. On average, we observe improvements of $4.45\times$, $2.82\times$, $1.74\times$, $1.60\times$, $1.15\times$, $1.35\times$ and $1.11\times$ on AU, DI, G3, HM, PR, ST and TT respectively.

gSOFA with limited memory space optimization includes all the space complexity optimizations, further along with an explicit restriction on the available memory space. Particularly, we enable out-of-core frontierQueue[], newFrontierQueue[], tracker[] and newTracker[] management, bubble removal and dynamic allocation. For the gigantic array that is shared by all the data structures, we limit its size to be 16, 10 and 5 GBs to demonstrate the performance robustness of gSOFA. This optimization will involve transferring data between CPU and GPU memories and other overheads, such as, checking the condition of memory overflow.

Figure 14 presents the execution time and space consumption trade-off. The general trend is that the performance drops along with the shrinking of allocated space. However, for majority of the datasets, gSOFA still performs better than CPU parallel symbolic factorization of SuperLU_DIST. Particularly, gSOFA with merely 5 GB (around 30% of the required space), the gSOFA performance decreases by $1.30\times$, $1.25\times$, $1.35\times$, $1.60\times$, $2.08\times$ and $2.74\times$, respectively, on AU, DI, HM, PR, ST and TT datasets. And they are still faster than the CPU parallel symbolic factorization. We also notice that for G3, gSOFA starts to perform worse than CPU parallel symbolic factorization when the space is reduced to 5GB. The reason is that the reduction of allowed memory envelop directly leads to the decrease of concurrent sources (i.e., #C), which significantly affects the performance of gSOFA. Note, enabling out-of-core gSOFA results in the overhead of checking whether the frontier queue overflows that is accounted as “gSOFA: Others” time in Figure 14.

Strong scalability. Figure 15 demonstrates strong scaling of gSOFA up to 1,000 GPUs. On relatively large datasets, AU, DI, PR, HM and G3, from 100 GPUs to 1,000 GPUs, gSOFA achieves nearly ideal speedups of $8.80\times$, $8.24\times$, $7.69\times$, $8.07\times$ and $6.67\times$, respectively. In addition, gSOFA can effectively use a number of GPUs that is not necessarily a power-of-two,

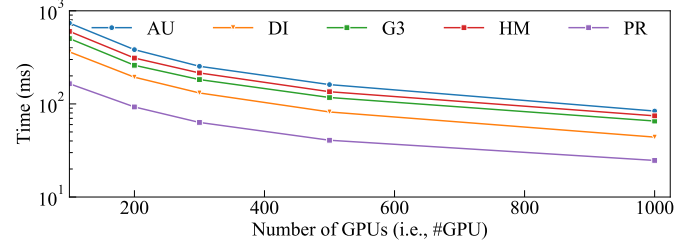


Figure 15: Scaling gSOFA to 1,000 GPUs.

which provides a great flexibility to the application code.

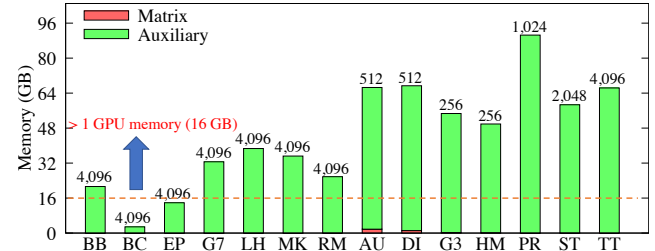


Figure 16: gSOFA memory consumption comparison of the original matrix and the auxiliary data structures in Table II. The number on top of each bar is the optimal #C per GPU for the corresponding dataset.

gSOFA GPU memory consumption. Figure 16 presents the GPU memory consumption for the sparse matrix and the auxiliary data structures mentioned in the Table II on one Summit node. One can observe that the memory requirement for the auxiliary data structures is orders of magnitude larger than that for the matrices. In particular, the maximum and minimum ratios of memory consumption for auxiliary data structure and matrices are 4222:1 in BB and 36:1 in AU, respectively. This motivates us to reduce the high space complexity requirement for the auxiliary data structures yet achieve similar performance as shown in Figure 14.

VIII. CONCLUSION AND FUTURE WORK

This paper introduces a scalable, fine-grained parallel symbolic factorization algorithm for GPUs. Particularly, we revamp the fill2 algorithm to enable fine-grained massively parallel symbolic factorization that is suitable for the SIMD nature of GPUs. To the best of our knowledge, this is the first attempt that scales symbolic factorization up to 1,000 GPUs.

As the future work, we plan to integrate GSOfA into state-of-the-art, i.e., SuperLU_DIST package.

REFERENCES

- [1] A. Azad, M. Jacquelin, A. Buluç, and E. G. Ng. The reverse cuthill-mckee algorithm in distributed-memory. In *2017 IEEE International Parallel and Distributed Processing Symposium (IPDPS)*, pages 22–31. IEEE, 2017.
- [2] X. Chen, L. Ren, Y. Wang, and H. Yang. Gpu-accelerated sparse lu factorization for circuit simulation with performance modeling. *IEEE Transactions on Parallel and Distributed Systems*, 26(3):786–795, 2014.
- [3] Y. Chen, T. A. Davis, W. W. Hager, and S. Rajamanickam. Algorithm 887: Cholmod, supernodal sparse cholesky factorization and update/downdate. *ACM Transactions on Mathematical Software (TOMS)*, 35(3):1–14, 2008.
- [4] S. S. M. Collection. Suite Sparse Matrix Collection. Retrieved from <https://sparse.tamu.edu/>. Accessed: 2019, November 15.
- [5] M. Cosnard and L. Grigori. A parallel algorithm for sparse symbolic lu factorization without pivoting on out-of-core matrices. In *Proceedings of the 15th international conference on Supercomputing*, pages 146–153. ACM, 2001.
- [6] E. Cuthill and J. McKee. Reducing the bandwidth of sparse symmetric matrices. In *Proceedings of the 1969 24th national conference*, pages 157–172, 1969.
- [7] T. A. Davis. *Direct methods for sparse linear systems*, volume 2. Siam, 2006.
- [8] T. A. Davis, S. Rajamanickam, and W. M. Sid-Lakhdar. A survey of direct methods for sparse linear systems. *Acta Numerica*, 25:383–566, 2016.
- [9] J. W. Demmel, S. C. Eisenstat, J. R. Gilbert, X. S. Li, and J. W. Liu. A supernodal approach to sparse partial pivoting. *SIAM Journal on Matrix Analysis and Applications*, 20(3):720–755, 1999.
- [10] E. W. Dijkstra et al. A note on two problems in connexion with graphs. *Numerische mathematik*, 1(1):269–271, 1959.
- [11] I. S. Duff. Parallel algorithms for sparse matrix solution. *Evans and Sutti [ES89]*, pages 73–82, 1989.
- [12] I. S. Duff. Ma57—a code for the solution of sparse symmetric definite and indefinite systems. *ACM Transactions on Mathematical Software (TOMS)*, 30(2):118–144, 2004.
- [13] I. S. Duff and J. Koster. The design and use of algorithms for permuting large entries to the diagonal of sparse matrices. *SIAM Journal on Matrix Analysis and Applications*, 20(4):889–901, 1999.
- [14] I. S. Duff and J. K. Reid. A comparison of some methods for the solution of sparse overdetermined systems of linear equations. *IMA Journal of Applied Mathematics*, 17(3):267–280, 1976.
- [15] I. S. Duff and J. K. Reid. *MA27-a set of Fortran subroutines for solving sparse symmetric sets of linear equations*. UKAEA Atomic Energy Research Establishment, 1982.
- [16] S. C. Eisenstat, M. Gursky, M. H. Schultz, and A. H. Sherman. Yale sparse matrix package i: The symmetric codes. *International Journal for Numerical Methods in Engineering*, 18(8):1145–1151, 1982.
- [17] S. C. Eisenstat and J. W. Liu. Exploiting structural symmetry in unsymmetric sparse symbolic factorization. *SIAM Journal on Matrix Analysis and Applications*, 13(1):202–211, 1992.
- [18] A. Gaihre, Z. Wu, F. Yao, and H. Liu. Xbfs: exploring runtime optimizations for breadth-first search on gpus. In *Proceedings of the 28th International Symposium on High-Performance Parallel and Distributed Computing*, pages 121–131, 2019.
- [19] A. George and J. W. Liu. Algorithms for matrix partitioning and the numerical solution of finite element systems. *SIAM Journal on Numerical Analysis*, 15(2):297–327, 1978.
- [20] A. George and E. Ng. A new release of sparspak: The waterloo sparse matrix package. *ACM SIGNUM Newsletter*, 19(4):9–13, 1984.
- [21] J. A. George. Computer implementation of the finite element method. Technical report, STANFORD UNIV CA DEPT OF COMPUTER SCIENCE, 1971.
- [22] J. A. George. Block elimination on finite element systems of equations. In *Sparse Matrices and Their Applications*, pages 101–114. Springer, 1972.
- [23] J. R. Gilbert and J. W. Liu. Elimination structures for unsymmetric sparse lu factors. *SIAM Journal on Matrix Analysis and Applications*, 14(2):334–352, 1993.
- [24] J. R. Gilbert and T. Peierls. Sparse partial pivoting in time proportional to arithmetic operations. *SIAM Journal on Scientific and Statistical Computing*, 9(5):862–874, 1988.
- [25] L. Grigori, J. W. Demmel, and X. S. Li. Parallel symbolic factorization for sparse lu with static pivoting. *SIAM Journal on Scientific Computing*, 29(3):1289–1314, 2007.
- [26] J. Huang and O. Wing. Optimal parallel triangulation of a sparse matrix. *IEEE Transactions on Circuits and Systems*, 26(9):726–732, 1979.
- [27] G. Karypis and V. Kumar. A parallel algorithm for multilevel graph partitioning and sparse matrix ordering. *Journal of Parallel and Distributed Computing*, 48(1):71–95, 1998.
- [28] B. W. Kernighan and S. Lin. An efficient heuristic procedure for partitioning graphs. *The Bell system technical journal*, 49(2):291–307, 1970.
- [29] C. P. Kruskal, L. Rudolph, and M. Snir. Techniques for parallel manipulation of sparse matrices. *Theoretical Computer Science*, 64(2):135–157, 1989.
- [30] K. Lab. ParMETIS. Retrieved from <http://glaros.dtc.umn.edu/gkhome/metis/parmetis/download>. Accessed: 2020, June 02.
- [31] D. LaSalle and G. Karypis. Multi-threaded graph partitioning. In *2013 IEEE 27th International Symposium on Parallel and Distributed Processing*, pages 225–236. IEEE, 2013.
- [32] D. LaSalle and G. Karypis. Efficient nested dissection for multicore architectures. In *European Conference on Parallel Processing*, pages 467–478. Springer, 2015.
- [33] X. S. Li and J. Demmel. A scalable sparse direct solver using static pivoting. In *PPSC*, 1999.
- [34] X. S. Li and J. W. Demmel. SuperLU_DIST: A scalable distributed-memory sparse direct solver for unsymmetric linear systems. *ACM Transactions on Mathematical Software (TOMS)*, 29(2):110–140, 2003.
- [35] H. Liu and H. H. Huang. Enterprise: breadth-first graph traversal on gpus. In *International Conference for High Performance Computing, Networking, Storage and Analysis*, pages 1–12. IEEE, 2015.
- [36] H. Liu, H. H. Huang, and Y. Hu. ibfs: Concurrent breadth-first search on gpus. In *Proceedings of the 2016 International Conference on Management of Data*, pages 403–416. ACM, 2016.
- [37] J. W. Liu. The multifrontal method for sparse matrix solution: Theory and practice. *SIAM review*, 34(1):82–109, 1992.
- [38] D. Merrill, M. Garland, and A. Grimshaw. Scalable gpu graph traversal. *Acm Sigplan Notices*, 47(8):117–128, 2012.
- [39] U. Meyer and P. Sanders. δ -stepping: a parallelizable shortest path algorithm. *Journal of Algorithms*, 49(1):114–152, 2003.
- [40] T. NVIDIA. Nvidia tesla v100 gpu architecture, 2017.
- [41] L. C. F. of Oak Ridge National Laboratory. Summit: America’s newest and smartest supercomputer. Retrieved from <https://www.olcf.ornl.gov/summit/>. Accessed: 2018, August 6.
- [42] A. Phillips. Gpu accelerated approach to numerical linear algebra and matrix analysis with cfd applications. 2014.
- [43] D. J. Rose. A graph-theoretic study of the numerical solution of sparse positive definite systems of linear equations. In *Graph theory and computing*, pages 183–217. Elsevier, 1972.
- [44] D. J. Rose and R. E. Tarjan. Algorithmic aspects of vertex elimination on directed graphs. *SIAM Journal on Applied Mathematics*, 34(1):176–197, 1978.
- [45] P. Sao, R. Kannan, P. Gera, and R. Vuduc. A supernodal all-pairs shortest path algorithm. In *Proceedings of the 25th ACM SIGPLAN Symposium on Principles and Practice of Parallel Programming*, pages 250–261, 2020.
- [46] E. Süli and D. F. Mayers. *An introduction to numerical analysis*. Cambridge university press, 2003.
- [47] M. Then, M. Kaufmann, F. Chirigati, T.-A. Hoang-Vu, K. Pham, A. Kemper, T. Neumann, and H. T. Vo. The more the merrier: Efficient multi-source graph traversal. *Proceedings of the VLDB Endowment*, 8(4):449–460, 2014.
- [48] W. F. Tinney and J. W. Walker. Direct solutions of sparse network equations by optimally ordered triangular factorization. *Proceedings of the IEEE*, 55(11):1801–1809, 1967.
- [49] Y. Wang, Y. Pan, A. Davidson, Y. Wu, C. Yang, L. Wang, M. Osama, C. Yuan, W. Liu, A. T. Riffel, et al. Gunrock: Gpu graph analytics. *ACM Transactions on Parallel Computing (TOPC)*, 4(1):1–49, 2017.